Available at www.sciencedirect.com

ScienceDirect

journal homepage: www.elsevier.com/locate/he

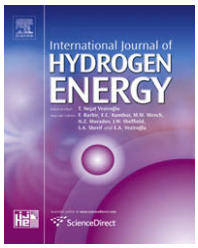

Structural and hydrogen storage properties of melt-spun Mg–Ni–Y alloys

Siarhei Kalinichenka[a], *Lars Röntzsch*[b,*], *Bernd Kieback*[a,b]

[a]*Institute for Materials Science, Technische Universität Dresden, 01069 Dresden, Germany*
[b]*Fraunhofer Institute for Manufacturing Technology and Applied Materials Research, Winterbergstrasse 28, 01277 Dresden, Germany*

ARTICLE INFO

Article history:
Received 29 May 2009
Received in revised form
17 July 2009
Accepted 17 July 2009
Available online 7 August 2009

Keywords:
Hydrogen storage material
Lightweight metal hydrides
Magnesium alloys
Melt spinning
Nanostructured material
Amorphous alloy

ABSTRACT

Nanocrystalline magnesium-rich Mg–Ni–Y alloys were produced by melt-spinning. They were characterized regarding their microstructure, crystallization behaviour, and cyclic hydrogenation/dehydrogenation properties in view of their application as reversible hydrogen storage materials. Transmission electron microscopy reveals that these alloys consist in the as-spun state of mixtures of nanocrystalline Mg(Ni;Y) grains that are embedded in an amorphous matrix. Differential scanning calorimetry and X-ray diffraction analysis show that these alloys undergo several crystallization steps in the temperature range between 180 and 370 °C. It was found that only a few thermal activation cycles of the as-quenched ribbons are required in order to reach excellent hydrogenation/dehydrogenation properties of these alloys. In thermogravimetric analyses using a magnetic suspension balance it could be shown that these alloys can reach reversible gravimetric hydrogen storage densities of up to 5.3 wt.%-H with hydrogenation and dehydrogenation rates of up to 1 wt.%-H/min even at temperatures of 250 °C. The structure of the alloys remains nanocrystalline even after several hydrogenation/dehydrogenation cycles.

1. Introduction

Magnesium hydride and magnesium alloy hydrides are very promising materials for the solid-state storage of hydrogen due to high gravimetric hydrogen storage densities of up to 7.6 wt.%-H in the case of MgH_2. Moreover, they are attractive for commercial use because of their cycle stability and the high abundance as well as the moderate cost of magnesium as lightweight base material [1]. Nevertheless, the slow hydrogen sorption kinetics and the high reactivity with humidity and oxygen are still challenges in view of practical applications.

In the last decade, increasing attention has been devoted to the research and development of novel magnesium-based alloys for hydrogen storage. It is now well established that, in order to enhance the hydrogen sorption kinetics, magnesium alloys should have a nanoscale crystal structure and should contain catalytically active elements such as transition metals, metal oxides, or rare earth elements [2]. For this purpose magnesium-rich alloys are commonly ground by high-energy ball-milling techniques to reduce the average grain size and to finely disperse catalyst particles [3–8]. Alternatively, nanocrystalline magnesium-rich alloys, which contain catalytic elements like transition metals or rare earths, can be produced by rapid solidification processes such as melt-spinning [9–14], where cooling rates can be expected in the range of 10^5–10^6 K/s [15]. With this high-yield rapid cooling technique, where material production rates in the range from 10^2 to 10^3 kg/h can be achieved in a single melt-spinning device, an amorphous or super-fine microstructure

* *Corresponding author*: Tel.: +49 351 2537 411; fax: +49 351 2537 399.
E-mail address: lars.roentzsch@ifam-dd.fraunhofer.de (L. Röntzsch).
0360-3199/$ – see front matter © 2009 Professor T. Nejat Veziroglu. Published by Elsevier Ltd. All rights reserved.
doi:10.1016/j.ijhydene.2009.07.053

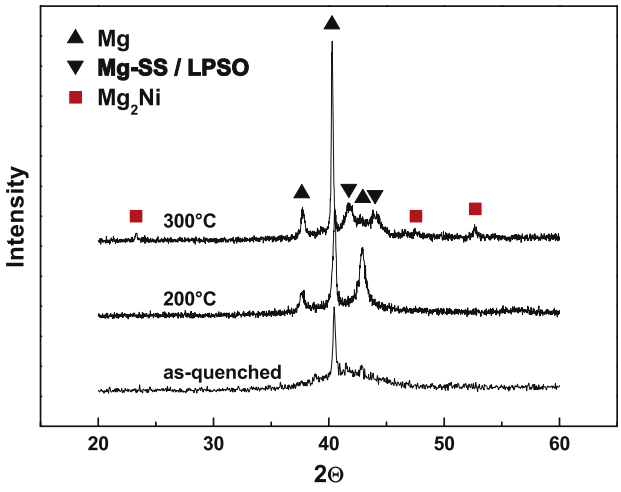

Fig. 1 – X-ray diffraction patterns of $Mg_{90}Ni_5Y_5$ in the as-quenched state and after crystallization at different temperatures.

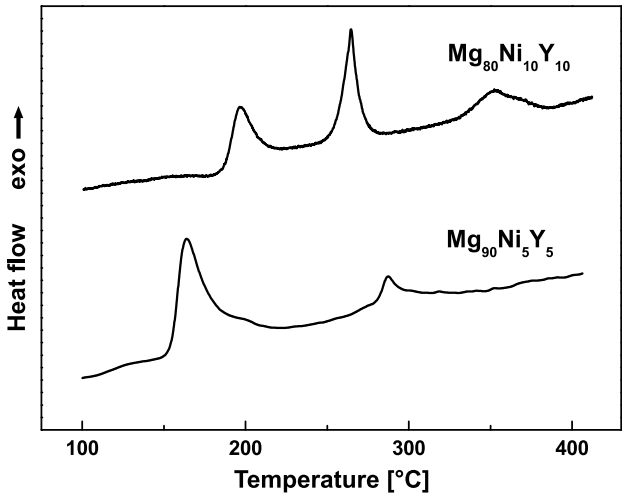

Fig. 3 – Crystallization behaviour of melt-spun $Mg_{80}Ni_{10}Y_{10}$ and $Mg_{90}Ni_5Y_5$ measured by DSC.

solidifies in the form of ribbons which are a few tens of micrometers thin.

In this work, two nanocrystalline magnesium-rich Mg–Ni–Y alloys ($Mg_{80}Ni_{10}Y_{10}$ and $Mg_{90}Ni_5Y_5$) were produced by melt-spinning. Their crystal structure, crystallization behaviour, and their cyclic hydrogenation/dehydrogenation properties were studied in view of their application as reversible hydrogen storage materials. This choice of alloy composition was used for several reasons: From the literature it is known that the addition of small amounts of nickel to magnesium significantly improves the hydrogenation/dehydrogenation kinetics and decreases the working temperature compared to that of pure magnesium [16–18]. Further, yttrium is widely known as glass-forming element in magnesium alloys [19]. On the other hand, ultrafine yttrium hydride particles, that are likely to form during hydrogenation of as-spun Mg–Ni–Y, improve the hydrogen sorption kinetics of magnesium [20]. Moreover, ultrafine crystal phases (like yttrium hydrides) can stabilize the nanostructure of magnesium-rich alloys by preventing further crystal coarsening during thermal processing, which could be very important in view of extensive hydrogenation/dehydrogenation cycling at elevated temperatures. Indeed, the produced Mg–Ni–Y alloys consist in the as-spun state of mixtures of nanocrystalline Mg(Ni;Y) grains with 5–20 nm in diameter that are embedded in an amorphous matrix as transmission electron microscopy (TEM) reveals. Differential scanning calorimetry (DSC) indicated that these alloys undergo several crystallization steps in the temperature range between 180 and 370 °C. It was found that only three thermal activation cycles of the as-quenched ribbons are required in order to reach excellent hydrogenation/dehydrogenation properties of these alloys. By thermogravimetric analysis (TGA) it could be shown that these alloys can reach reversible gravimetric hydrogen storage densities of up to 5.3 wt.%-H with hydrogenation and dehydrogenation rates of up to 1 wt.%-H/min even at temperatures of 250 °C. Presumably due to the yttrium content of the alloy, which triggers the formation of highly disperse yttrium hydride phases, the structure of the alloys remains nanocrystalline even after several hydrogenation/dehydrogenation cycles.

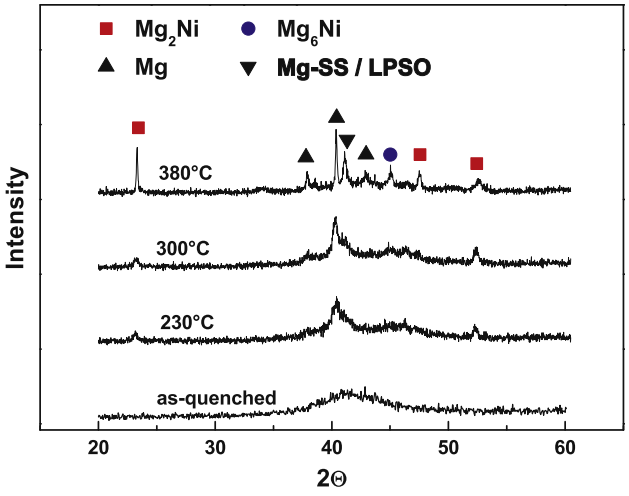

Fig. 2 – X-ray diffraction patterns of $Mg_{80}Ni_{10}Y_{10}$ in the as-quenched state and after crystallization at different temperatures.

2. Experimental

2.1. *Materials and preparation methods*

Mg–Ni–Y master alloy ingots with two different chemical compositions ($Mg_{90}Ni_5Y_5$ and $Mg_{80}Ni_{10}Y_{10}$) were produced by induction-melting of a mixture of pure Mg (99.9% purity) metal, Ni (99.9% purity) powder, and a Ni–Y (Ni – 25.4 wt.%; Y – 75.5 wt.%) alloy in a tantalum crucible under argon atmosphere. During melt-spinning of these alloys, continuous ribbons with 35 μm in thickness and 10 mm in width were

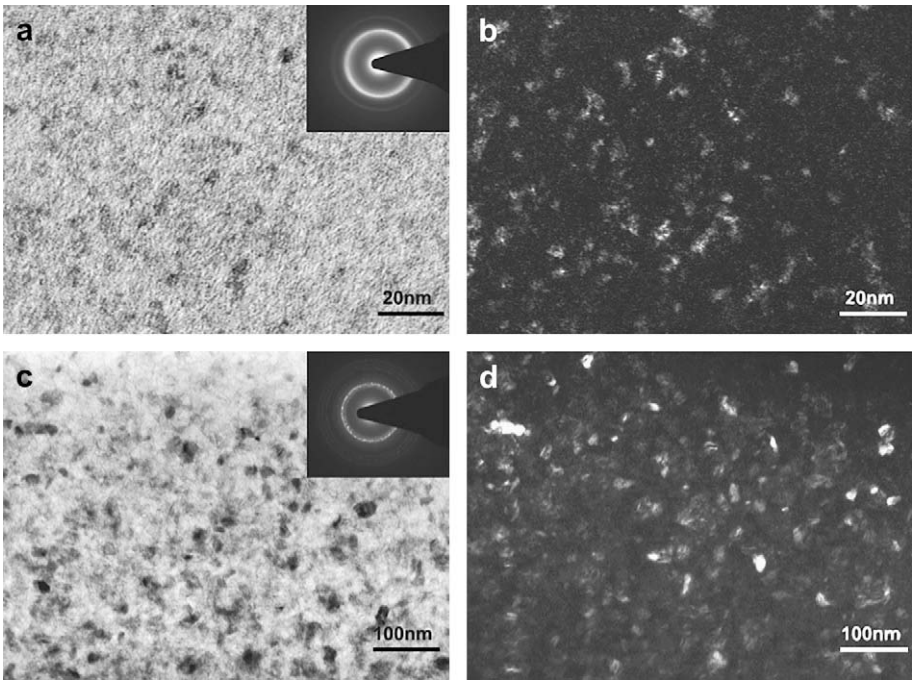

Fig. 4 – TEM micrographs of as-spun Mg–Ni–Y alloys with the corresponding selected-area electron diffraction patterns: (a, b) $Mg_{80}Ni_{10}Y_{10}$ and (c, d) $Mg_{90}Ni_5Y_5$.(a, c) bright-field imaging mode and (b, d) dark-field imaging mode.

obtained from a single roller melt-spinning device (PSI) which contains a copper wheel with a diameter of 200 mm and a constant surface velocity of 40 m/s as rapid cooling component. The melt-spinning experiments were carried our under argon atmosphere. Since it is well known from the literature that the melt-spun ribbons should be activated prior to hydrogenation [11, 12, 17], the thermal activation of the melt-spun ribbons was carried out for three cycles at 350 °C and pressures between 2 and 30 bar H_2 for 11 h.

2.2. *Analysis*

The crystal structure characterization of the samples has been performed by X-ray diffraction analysis (XRD, D5000 Siemens) using Co Kα radiation in the scanning range of the diffraction angle between 10° and 100° (2Θ). The spectra were analyzed with the Rietveld method [21], using the software package Topas 4.2 for the refinement of crystal structures and the calculation of the unit cell parameters as well as the phase abundances.

The thermal characteristics of the melt-spun ribbons were studied by DSC analysis (Netzsch DSC 404) for the melt-spun alloys at a heating rate of 10 K/min in argon atmosphere at ambient pressure.

The microstructure characterization of the specimens has been carried out using an EVO 50 ZEISS scanning electron microscope (SEM) and a FEI Tecnai G2 F20 TEM. For TEM

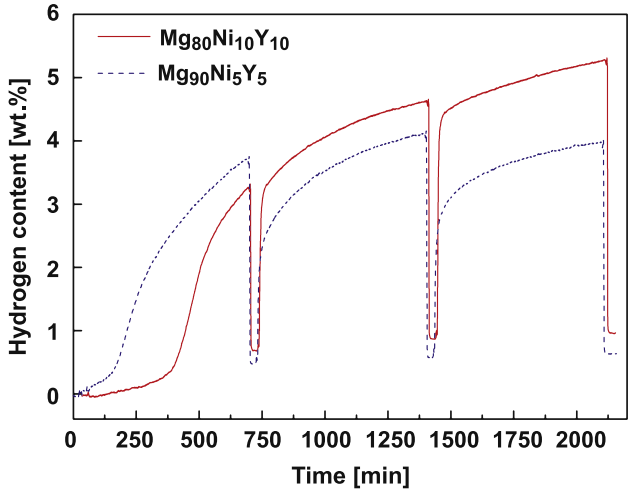

Fig. 5 – The three activation cycles of melt-spun Mg–Ni–Y ribbons (at 350 °C; 30/2 bar H_2 for 11/0.5 h).

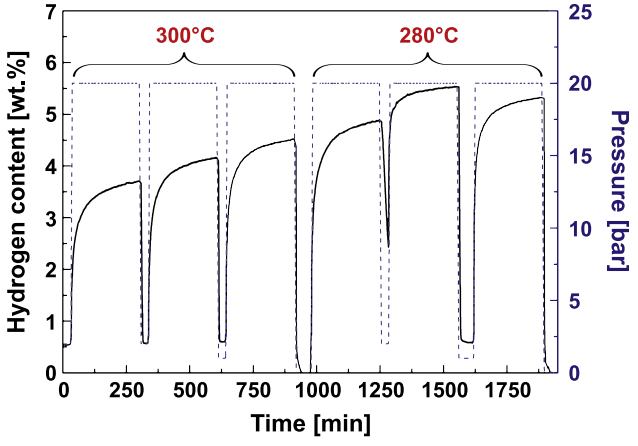

Fig. 6 – Hydrogenation/dehydrogenation behaviour of the melt-spun and activated $Mg_{90}Ni_5Y_5$ alloy at 300 and 280 °C and at 20 bar H_2 (hydrogenation) and 2/1/0 bar H_2 (dehydrogenation).

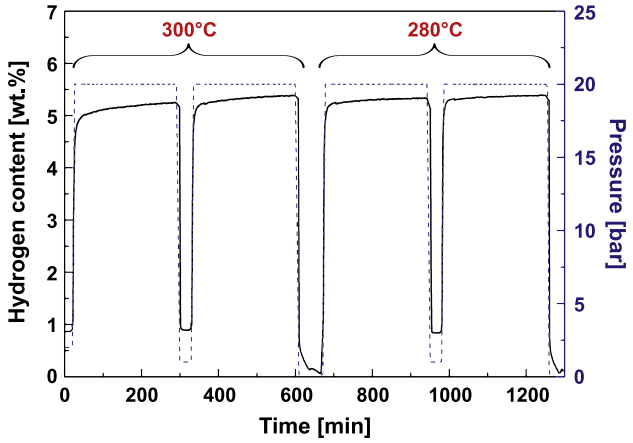

Fig. 7 – Hydrogenation/dehydrogenation behaviour of the melt-spun and activated $Mg_{80}Ni_{10}Y_{10}$ alloy at 300 and 280 °C and at 20 bar H_2 (hydrogenation) and 1/0 bar H_2 (dehydrogenation).

observations, the as-spun Mg–Ni–Y ribbons were ion milled for 10 h with an ion-milling system (BAL-TEC RES 101). For the TEM study of the hydrogenated alloys, the samples were ground into fine powders by adding ethanol and were dispersed thereafter on a copper micro-grid.

The hydrogenation/dehydrogenation properties (reaction kinetics) and cycle stability of the melt-spun Mg–Ni–Y ribbons were studied using a magnetic suspension balance (Rubotherm). Therefore, hydrogen desorption can be investigated at constant hydrogen partial pressures in the range from 10^{-3} to 10^{1} bar, i.e. covering the operating pressure range of most proton-exchange membrane fuel cell systems.

3. Results and discussion

3.1. *Structural characterization of as-spun and crystallized Mg–Ni–Y ribbons*

The XRD patterns of the as-spun $Mg_{90}Ni_5Y_5$ and $Mg_{80}Ni_{10}Y_{10}$ ribbons are shown in Figs. 1 and 2. It can be seen that the as-quenched $Mg_{80}Ni_{10}Y_{10}$ ribbon shows a typical amorphous structure. $Mg_{90}Ni_5Y_5$ ribbons consist of Mg crystals embedded in an amorphous Mg–Ni–Y phase (0 0 2)-peak at 40° (2Θ).

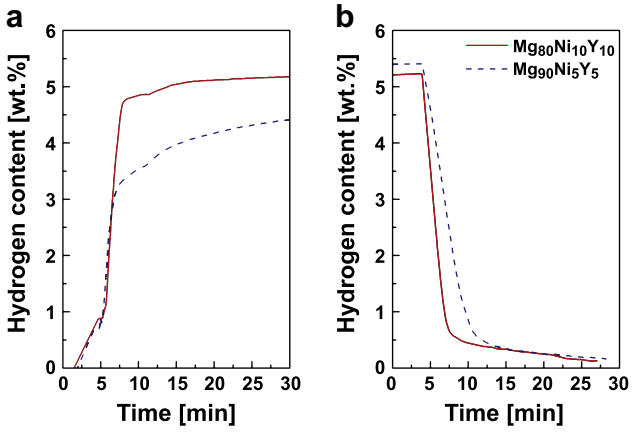

Fig. 8 – Hydrogen content vs. time of the activated Mg–Ni–Y ribbons at 250 °C for (a) hydrogen absorption at 20 bar H_2 and (b) hydrogen desorption in vacuum.

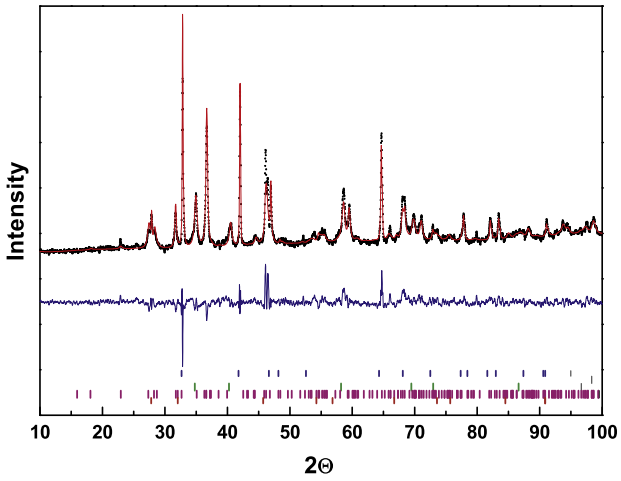

Fig. 9 – Calculated (line) and measured (*) X-ray diffraction pattern for $Mg_{80}Ni_{10}Y_{10}$ in the hydrogenated state together with difference and *hkl* markers for MgH_2, YH_3, YH_2, and Mg_2NiH_4 (monoclin/cubic).

The crystallization temperatures of the as-spun Mg–Ni–Y ribbons were determined by DSC measurements, which displayed two and three exothermic peaks for $Mg_{90}Ni_5Y_5$ and $Mg_{80}Ni_{10}Y_{10}$, respectively (cf. Fig. 3). It can be seen that the crystallization of the as-quenched Mg–Ni–Y alloys consists of several steps and that $Mg_{80}Ni_{10}Y_{10}$ has higher thermal stability compared to $Mg_{90}Ni_5Y_5$. The structure characterization of $Mg_{80}Ni_{10}Y_{10}$ using XRD showed that the first crystallization reaction at 200 °C is the crystallization of Mg_2Ni phase and is connected with the first exothermic DSC peak (cf. Fig. 3). The residual amorphous phase is stable even after the second crystallization step at 280 °C and transforms mainly into Mg at

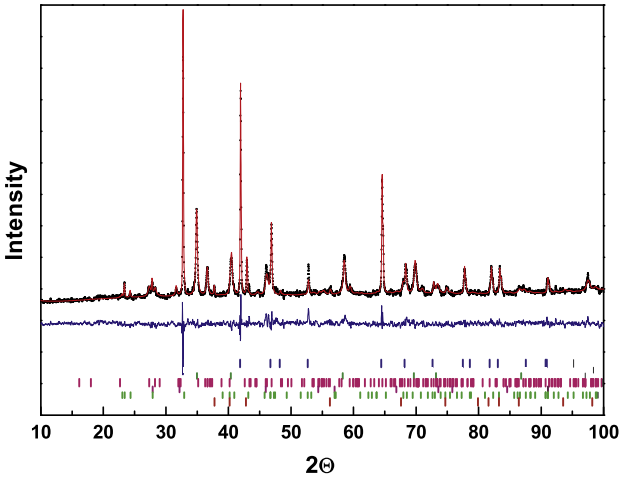

Fig. 10 – Calculated (line) and measured (*) X-ray diffraction pattern for $Mg_{90}Ni_5Y_5$ in the hydrogenated state together with difference and *hkl* markers for MgH_2, YH_3, YH_2, Mg_2NiH_4 (monoclin/cubic), $Mg_2NiH_{0.3}$, and Mg.

Table 1 – Phase abundance of the of hydrogenated melt-spun Mg–Ni–Y alloys refined by the Rietveld analysis.

Sample	Phase	Space group	Lattice parameters			Abundance (wt.%)
			a (Å)	*b* (Å)	*c* (Å)	
$Mg_{80}Ni_{10}Y_{10}$, $R_{WP} = 11.25\%$	MgH_2	$P4_2/mnm$	4.5194		3.0230	35.47
	YH_3	*P-3c1*	6.3606		6.6137	11.82
	YH_2	*Fm-3 m*	5.207			12.41
	LT-Mg_2NiH_4	*C2/c*	14.4027	6.4044	6.5126	34.5
	HT-Mg_2NiH_4	*Fm-3 m*	6.5070			5.80
$Mg_{90}Ni_5Y_5$, $R_{WP} = 10.52\%$	MgH_2	$P4_2/mnm$	4.5154		3.0239	52.62
	YH_3	*P-3c1*	6.3548		6.6033	6.1
	YH_2	*Fm-3 m*	5.1946			16.06
	LT-Mg_2NiH_4	*C2/c*	14.315	6.4432	6.5122	16.35
	HT-Mg_2NiH_4	*Fm-3 m*	6.5004			2.25
	$Mg_2NiH_{0.3}$	$P6_222$	5.23052		13.3678	4.52
	Mg	$P6_3/mmc$	3.21117		5.2159	2.1

380 °C (the third exothermal DSC peak). Furthermore, a minority crystal phase with a smaller lattice parameter than Mg is observed (cf. Figs. 1 and 2) which we suggest could either be a Mg solid-solution (Mg-SS) phase or a Mg long-period stacking ordered (LPSO) structure. The suggested Mg-SS phase has smaller lattice parameters than pure Mg which could be caused by the substitution of Mg by Ni or Y or both. The LPSO phase is characterized by a (Y,Ni)-plane that is intercalated between a sequence of pure Mg planes [22]. The precise nature of this particular phase needs to be revealed in further studies. In our XRD investigations we have not observed the formation of Ni–Y or Mg–Y intermetallics in any sample. Also, we can exclude any oxide formation of the constituents.

In Fig. 4, the microstructure of the as-spun Mg–Ni–Y alloys observed by TEM is presented, together with their electron diffraction patterns. The microstructure was mainly composed of a considerable amount of nanocrystalline phases of Mg(Ni,Y) crystals which are embedded in an amorphous phase. The average crystal size was about 20 nm in the case of $Mg_{90}Ni_5Y_5$ and about 5 nm in the case of $Mg_{80}Ni_{10}Y_{10}$.

3.2. *Hydrogenation and dehydrogenation properties of melt-spun Mg–Ni–Y*

In Fig. 5, the three activation cycles of the as-spun $Mg_{90}Ni_5Y_5$ and $Mg_{80}Ni_{10}Y_{10}$ ribbons are shown. The hydrogenation and dehydrogenation were carried out at 350 °C under 30 bar H_2 for 11 h and under 2 bar H_2 for 30 min, respectively. Evidently, in the case of $Mg_{80}Ni_{10}Y_{10}$ significant hydrogen absorption occurs after 380 min and the activation lasts three cycles to achieve a maximum content of hydrogen of about 5.3 wt.%-H. The activation of as-spun $Mg_{90}Ni_5Y_5$ alloy takes place in the first activation cycle, and no further improvement of the hydrogen absorption could be observed during the following cycles. This behaviour can be explained by the higher thermal stability of melt-spun $Mg_{80}Ni_{10}Y_{10}$ (crystallization at higher temperatures) compared to $Mg_{90}Ni_5Y_5$ (cf. Fig. 3). It can also be established that $Mg_{80}Ni_{10}Y_{10}$ as well as $Mg_{90}Ni_5Y_5$ do not completely desorb the formerly absorbed hydrogen at 350 °C and at 2 bar hydrogen partial pressure. The reason can be attributed to the formation of the stable hydrides like yttrium hydrides, for example (cf. Fig. 8).

After the activation treatment described above, the characterization of the hydrogenation and dehydrogenation properties of activated Mg–Ni–Y alloys was carried out at different temperatures of 300, 280, and 250 °C. Fig. 6 shows the hydrogen content and the applied system hydrogen pressure vs. time of the activated $Mg_{90}Ni_5Y_5$ alloy for the absorption of hydrogen at 300 and 280 °C with an initial system pressure of 20 bar H_2 and the desorption of hydrogen at 300 and 280 °C at pressures of 2 bar H_2, 1 bar H_2, and in vacuum, respectively. Obviously, the gravimetric hydrogen-storage density of $Mg_{90}Ni_5Y_5$ alloy continues to increase with the number of cycles and achieves 5.3 wt.%-H at 280 °C. It can also be recognized that $Mg_{90}Ni_5Y_5$ alloy does not desorb the formerly absorbed hydrogen at 300 and 280 °C at 2 bars and 1 bar H_2 completely. The complete desorption can be achieved only in vacuum. The fact that the H-absorption capacity decreases between the second and the third cycle at 280 °C can be explained by the different initial states of the sample prior to each cycle. After the first cycle the sample did not desorb completely in comparison to the second cycle at 280 °C.

Fig. 7 depicts the hydrogen content and the hydrogen pressure vs. time of the activated $Mg_{80}Ni_{10}Y_{10}$ alloy for the absorption of hydrogen at 300 and 280 °C at a partial pressure of 20 bar H_2 as well as the desorption of hydrogen at 300 and 280 °C at a partial pressure of 1 bar H_2 and in vacuum. As in the case of the activated $Mg_{90}Ni_5Y_5$ alloy, the activated $Mg_{80}Ni_{10}Y_{10}$ alloy does not desorb the formerly absorbed hydrogen completely, and the residual hydrogen can only be removed in vacuum. However, it can also absorb up to 5.3 wt.%-H at 280 °C and at a pressure of 20 bar H_2.

The hydrogenation rates of the studied alloys are high at pressures of 20 bar H_2, even at 250 °C (cf. Fig. 8), i.e. they can reach rates of up to 1 wt.%-H/min, while the hydrogen desorption rates at 250 °C slow down below 1 bar H_2, and a complete hydrogen desorption can be observed only in vacuum. Obviously, in Fig. 8, the hydrogen content for $Mg_{90}Ni_5Y_5$ is lower on absorption than the initial concentration on desorption which is due to the fact that only the first 30 min of the processes are depicted. However, the desorption was carried out after the full hydrogen capacity was reached after approximately 4 h.

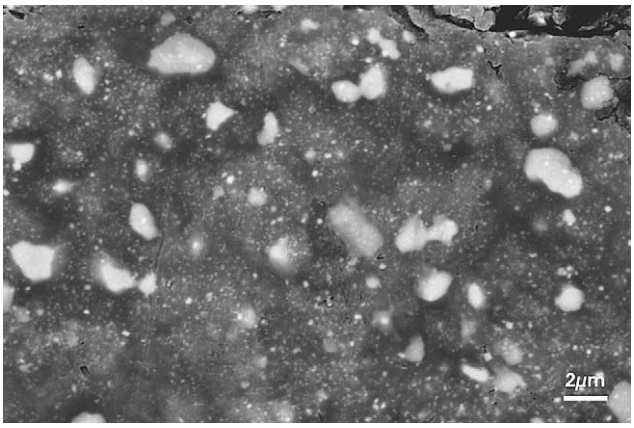

Fig. 11 – SEM micrograph of hydrogenated $Mg_{90}Ni_5Y_5$ ribbon after 10.5 h/d cycles (details see text).

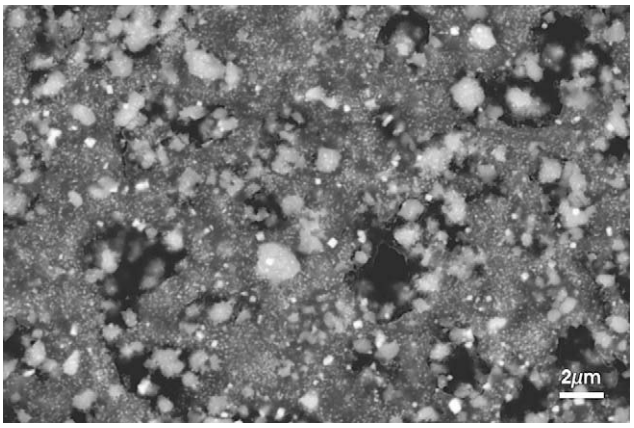

Fig. 12 – SEM micrograph of hydrogenated $Mg_{80}Ni_{10}Y_{10}$ ribbon after 10.5 h/d cycles (details see text).

In addition, it can also be noticed that especially at temperatures below 300 °C the hydrogenation and dehydrogenation rates of $Mg_{80}Ni_{10}Y_{10}$ are higher than that of $Mg_{90}Ni_5Y_5$. These differences in the hydrogenation behaviour have to be associated with the different composition of the alloys as well as with the differences in their microstructure in the as-spun and hydrogenated state (cf. Figs. 4, 11, and 12). The higher hydrogenation rates of the $Mg_{80}Ni_{10}Y_{10}$ could be explained by its higher yttrium and nickel content. Yttrium is known to form very stable hydrides which act as catalysts for the hydrogenation of magnesium [20, 24]. Furthermore, yttrium can be solved in Mg_2Ni. In addition, yttrium possesses a larger atomic radius compared to nickel, thus yttrium increases the lattice parameter of Mg_2Ni to a certain extent which might lead to faster hydrogen diffusion in the Mg_2Ni phase [23]. Likewise, the existence of Mg_2NiH_4 also plays a catalytic role for the hydrogenation of magnesium [16, 17].

3.3. *Microstructure and morphology of hydrogenated alloys*

Figs. 9 and 10 show XRD diffraction spectra of the hydrogenated melt-spun Mg–Ni–Y alloys. The results of Rietveld analysis indicate that the hydrogenated $Mg_{80}Ni_{10}Y_{10}$ sample contains five different hydride phases (cf. Table 1): MgH_2, high-temperature (HT) and low-temperature (LT) Mg_2NiH_4, YH_2, and YH_3. The hydrogenated $Mg_{90}Ni_5Y_5$ ribbon contains additionally Mg and $Mg_2NiH_{0.3}$. These phases occurred probably due to incomplete hydrogenation of the sample and suggest a deficiency effect of the catalyst particles.

The SEM micrographs (backscattered electron imaging mode) in Figs. 9 and 10 show the corresponding hydrogenated microstructures of the melt-spun ribbons after 10.5 hydrogenation/dehydrogenation cycles. It can be stated that the ribbons basically retained their original structure even after 10 cycles. They were very brittle and could be powderized easily. As shown in Figs. 9 and 10, the microstructure of ribbons in the hydrogenated state consisted mainly of coarse Mg_2NiH_4 grains with 1–2 μm in size and of nanocrystalline yttrium hydride particles embedded in a MgH_2 matrix whose average crystal size is in the range of 100 nm (TEM results, not shown). From TEM investigations of the ribbons, the average size of yttrium hydride particles is determined to be about 50 nm. It can also be observed that the $Mg_{90}Ni_5Y_5$ sample contains coarser grains of Mg_2NiH_4 in comparison to $Mg_{80}Ni_{10}Y_{10}$. This can also be explained by the higher yttrium content in $Mg_{80}Ni_{10}Y_{10}$. In other words, nanoscale yttrium hydride phases very obviously stabilize the nanostructure of the Mg–Ni–Y alloys during thermal treatments.

In the literature, there are only a few investigations on the hydrogenation kinetics of magnesium-rich Mg–Ni–Y alloys. For example, Spassov et al. [9, 10] reported results of hydrogen storage properties of the various nanocrystalline and nanoamorphous Mg–Ni–Y alloys ($Mg_{87}Ni_{12}Y_1$, $Mg_{63}Ni_{30}Y_7$, $Mg_{76}Ni_{19}Y_5$, $Mg_{78}Ni_{18}Y_4$, and $Mg_{83}Ni_{9.5}Y_{7.5}$) produced by rapid solidification. In contrast to the results obtained in this study, the hydrogen charging of the ribbons was carried out by Spassov and co-workers electrolytically under galvanostatic conditions, and the amount of hydrogen was determined from the sample mass after hydrogenation. They found that these Mg–Ni–Y alloys show rather slow rate of hydrogen absorption (0.15–0.3 wt.%-H/min) and a maximum gravimetric hydrogen capacity of about 3.2 wt.%-H. In Ref. [24] the hydrogen sorption properties of Mg-20 wt.% Ni–Y composites prepared by reactive mechanical alloying were studied after the total milling time of 40 h. The hydrogen sorption behaviour of the composites was evaluated using a conventional volumetric method. This composite does not need activation for hydrogen storage process and it can absorb 5.59 wt.%-H at pressures of 30 bar H_2 at 200 °C in 10 min and desorb 4.67 wt.%-H at 250 °C in 30 min at a hydrogen pressure of 0.2 bar. Compared to these values, the Mg–Ni–Y alloys investigated in this study exhibit even higher hydrogen storage capacities and faster hydrogenation/dehydrogenation kinetics. Nonetheless, there is still a need for decreasing the temperatures of hydrogen desorption which could be achieved by catalytically more active elements, for example.

4. Conclusion

Structural and hydrogen storage properties of two melt-spun Mg–Ni–Y alloys ($Mg_{90}Ni_5Y_5$ and $Mg_{80}Ni_{10}Y_{10}$) were studied by TEM, SEM, XRD, DSC, and TGA. The as-quenched alloys were found to consist mainly of Mg(Ni,Y) nanocrystals, with an average size between 5 and 20 nm embedded in an amorphous matrix. The as-quenched Mg–Ni–Y ribbons were activated during the three hydrogenation/dehydrogenation cycles at 350 °C and 30/2 bar H_2. It was found that the activation behaviour of melt-spun alloys is different. The $Mg_{80}Ni_{10}Y_{10}$ sample shows generally higher thermal stability and higher hydrogenation rates compared to the $Mg_{90}Ni_5Y_5$ alloy. The activated $Mg_{90}Ni_5Y_5$ and $Mg_{80}Ni_{10}Y_{10}$ absorb about 5.3 wt.%-H at 280 °C under 20 bar H_2. The hydrogenation rates and the maximum hydrogen storage capacity of the alloys are quite high, even at 250 °C, while the dehydrogenation rates at 250 °C slow down at 1 bar H_2, thus full hydrogen desorption can be achieved only in vacuum thus far. The microstructure of the hydrogenated melt-spun ribbons contained nanocrystalline yttrium hydride particles in the MgH_2 phase even after 10 hydrogenation/dehydrogenation cycles. In conclusion, the melt-spinning technique is very effective in obtaining nanocrystalline magnesium-rich and catalytically activated alloys. In this respect, the present study suggests that the Mg–Ni–Y system is very suitable for the reversible solid-state storage of hydrogen.

Acknowledgements

The authors would like to acknowledge the financial support of the Boysen-Stiftung and the Fraunhofer Attract program. Further, the authors thank Chr. Mickel (IFW Dresden) very much for TEM analyses and sample preparation. They are also grateful to R. Leuschner, V. Pacheco, and M. Ruhnow for their practical support.

REFERENCES

[1] Schlapbach L, Zuettel A. Hydrogen-storage materials for mobile applications. Nature 2001;414:353–8.
[2] Fichtner M. Nanotechnological aspects in materials for hydrogen storage. Adv Eng Mater 2005;7:443–55.
[3] Gutfleisch O, Dal Toè S, Herrich M, Handstein A, Pratt A. Hydrogen sorption properties of Mg–1 wt.% Ni–0.2 wt.% Pd prepared by reactive milling. J Alloys Compd 2005;404–406: 413–6.
[4] Liang G, Huot J, Boily S, Van Neste A, Schulz R. Catalytic effect of transition metals on hydrogen sorption in nanocrystalline ball milled MgH_2–Tm (Tm = Ti, V, Mn, Fe and Ni) systems. J Alloys Compd 1999;292:247–52.
[5] Bystrzycki J, Czujko T, Varin RA. Processing by controlled mechanical milling of nanocomposite powders Mg + X (X = Co, Cr, Mo, V, Y, Zr) and their hydrogenation properties. J Alloys Compd 2005;404–406:507–10.
[6] Gennari FC, Esquivel MR. Structural characterization and hydrogen sorption properties of nanocrystalline Mg_2Ni. J Alloys Compd 2008;459:425–32.
[7] Shang CX, Bououdina M, Song Y, Guo ZX. Mechanical alloying and electronic simulations of (MgH_2 + M) systems (M = Al, Ti, Fe, Ni, Cu and Nb) for hydrogen storage. Int J Hyd Energy 2004;29:73–80.
[8] Bobet J-L, Akiba E, Darriet B. Study of Mg–M (M = Co, Ni and Fe) mixture elaborated by reactive mechanical alloying: hydrogen sorption properties. Int J Hyd Energy 2001;26. 493–01.
[9] Spassov T, Koster U. Thermal stability and hydriding properties of nanocrystalline melt-spun $Mg_{63}Ni_{30}Y_7$ alloy. J Alloys Compd 1998;279:279–86.
[10] Spassov T, Lyubenova U, Köster U, Barò MD. Mg–Ni–RE nanocrystalline alloys for hydrogen storage. Mater Sci Eng A 2004;375–377:794–9.
[11] Tanaka K, Kanda Y, Furuhashi M, Saito K, Kuroda K, Saka H. Improvement of hydrogen storage properties of melt-spun Mg–Ni–RE alloys by nanocrystallization. J Alloys Compd 1999; 293–295:521–5.
[12] Song MY, Kwon S, Bae J-S, Hong S- H. Hydrogen-storage properties of Mg–23.5 Ni–(0 and 5) Cu prepared by melt spinning and crystallization heat treatment. Int J Hyd Energy 2008;33:1711–8.
[13] Wu Y, Solberg JK, Yartys VA. The effect of solidification rate on microstructural evolution of a melt-spun Mg–20Ni–8Mm hydrogen storage alloy. J Alloys Compd 2008;446:178–82.
[14] Tanaka K, Miwa T, Sasaki K, Kuroda K. TEM studies of nanostructure in melt-spun Mg–Ni–La alloy manifesting enhanced hydrogen desorbing kinetics. J Alloys Compd 2009; 478:308–16.
[15] Suryanarayana C, editor. Non-equilibrium processing of materials. Oxford: Pergamon; 1999.
[16] Reilly JJ, Wiswall RH. The reaction of hydrogen with alloys of magnesium and nickel and the formation of Mg_2NiH_4. J Inorg Chem 1968;7:2254–6.
[17] Friedlmeier G, Arakawa M, Hirai T, Akiba E. Preparation and structural, thermal and hydriding characteristics of melt-spun Mg–Ni alloys. J Alloys Compd 1999;292:107–17.
[18] Yim CD, You BS, Na YS, Bae JS. Hydriding properties of Mg– xNi alloys with different microstructures. Catal Today 2007;120:276–80.
[19] Kim SG, Inoue A, Masumoto T. High mechanical strengths of Mg–Ni–Y and Mg–Cu–Y amorphous alloys with significant supercooled liquid region. Mater Trans JIM 1990;31:929–34.
[20] Orimo S, Fujii H, Tabata M. Synthesis of fine composite particles for hydrogen storage, starting from Mg–YNi_2 mixture. J Alloys Compd 1994;210:37–43.
[21] Young RA, editor. The Rietveld method. Oxford: Oxford University Press; 1993.
[22] Garces G, Perez P, Gonzales S, Adeva P. Development of long-period ordered structures during crystallisation of amorphous $Mg_{80}Cu_{10}Y_{10}$ and $Mg_{83}Ni_9Y_8$. Int J Mater Res 2006; 97:404–8.
[23] Cui N, Luan B, Zhao HJ, Liu HK, Dou SX. Effects of yttrium additions on the electrode performance of magnesium-based hydrogen storage alloys. J Alloys Compd 1996;233:236–40.
[24] Li Z, Liu X, Jiang L, Wang S. Characterization of Mg–20 wt% Ni–Y hydrogen storage composite prepared by reactive mechanical alloying. Int J Hyd Energy 2007;32:1869–74.